PHYSICAL REVIEW A **79**, 021605(R) (2009)

# Technique for measuring atomic recoil frequency using coherence functions

S. Beattie,[1] B. Barrett,[1] I. Chan,[1] C. Mok,[1] I. Yavin,[2] and A. Kumarakrishnan[1]
[1]*Department of Physics and Astronomy, York University, Toronto, Ontario M3J 1P3, Canada*
[2]*Joseph Henry Laboratories, Princeton University, Princeton, New Jersey 08544, USA*
(Received 2 July 2008; revised manuscript received 7 November 2008; published 13 February 2009)

We have developed a technique for measuring the atomic recoil frequency using a single-state echo-type atom interferometer that manipulates laser-cooled atoms in the ground state. The interferometer relies on momentum-state interference due to two standing-wave pulses that produce density gratings. The interference is modified by applying a third standing-wave pulse during the interferometer pulse sequence. As a result, the grating contrast exhibits periodic revivals at the atomic recoil frequency $\omega_r$ as a function of the time at which the third pulse is applied, allowing $\omega_r$ to be measured easily and precisely. The contrast is accurately described by a coherence function, which is the Fourier transform of the momentum distribution, produced by the third pulse and by the theory of echo formation. If the third pulse is a traveling wave, loss of grating contrast is observed, an effect also described by a coherence function. The decay of the grating contrast as a function of continuous-wave light intensity is used to infer the cross section for photon absorption.

DOI: 10.1103/PhysRevA.79.021605 PACS number(s): 03.75.Dg, 37.10.Jk, 37.10.Vz, 42.50.Md

Following the demonstration of diffraction of atoms by standing-wave laser fields [1], atom interferometers (AIs) involving laser-cooled atoms have achieved significant improvements in inertial sensing [2,3] and contributed to improved measurements of the atomic fine-structure constant $\alpha$ [4–6]. AIs using cold atoms have generally relied on Raman transitions between hyperfine ground states [2–5], whereas AIs used for studies of decoherence [7–10] have utilized microfabricated gratings and supersonic atomic beams to observe effects of spatially separated laser fields on momentum-state interference. The results of beam experiments have been interpreted on the basis of coherence functions in classical optics associated with traveling-wave pulses [11]. This paper describes a technique for measuring the atomic recoil frequency using a single-state, time-domain AI that utilizes the coherence function associated with a standing-wave pulse.

The AI uses a cold gas of Rb atoms and an echo technique that was previously developed in Refs. [12–17]. The sample is excited by two standing-wave pulses (with traveling-wave components far detuned from the excited state) turned on at $t=0$ and $t=T$ that satisfy the Raman-Nath criterion [see Fig. 1(a)]. Each pulse transfers momenta in integer multiples $2n\hbar k$ due to absorption and stimulated emission of photons, where $k=2\pi/\lambda$ is the wave vector of the traveling-wave components of the standing wave. After excitation, the sample evolves into a superposition of momentum states corresponding to the same internal ground state. The recoil phases of the momentum states scale as $n^2\omega_r$ where $\omega_r=\hbar\Delta k^2/2m$ is the atomic recoil frequency, $m$ is the atomic mass, and $\Delta k=2k$ is the momentum transfer from counterpropagating excitation beams. The Doppler phases of these states evolve as $n\Delta k v_0 t$ where $v_0$ is the initial atomic velocity. The modulation of the wave function occurs on a time scale $T_r=\frac{\pi}{\omega_r}$ ($\sim 32\ \mu$s), which is much greater than the Doppler dephasing time $T_D\sim 1/ku$ ($\sim 1\ \mu$s) for a sample temperature of 50 $\mu$K. Here $u$ is the most probable speed of the atomic cloud. Therefore, it is necessary to use the echo technique to observe the recoil modulation of the wave function. The phase modulation after the first standing-wave pulse evolves into a density grating on a time scale $T_r$. Interaction with the second standing-wave pulse results in the interference of momentum states separated by $2\hbar k$ at the echo time $t=2T$, at which the Doppler-phase differences between interfering momentum states cancel. A rephased density grating with period $\lambda/2$ formed in the vicinity of this echo time can be detected by coherently backscattering a traveling-wave readout pulse with wavelength $\lambda$. The amplitude of the backscattered light (echo) as a function of standing-wave pulse separation, $T$, is a direct measure of the grating contrast and exhibits a modulation at $\omega_r$ because atoms with recoil velocity $2\hbar k/m$ are displaced by one grating period ($\lambda/2$) in time $T_r$.

In this paper, we investigate the effects of a third pulse applied at $t=2T-\delta T$ on the echo at $t=2T$. In contrast with beam experiments, all atoms interact with all pulses for the same duration and $\delta T$ can be varied easily and with exquisite control. If the third pulse is a standing wave similar to the two AI pulses, the effect of spontaneous emission is minimal. The contrast at $t=2T$ can be completely recovered when $\delta T$ is an integer multiple of $T_r$ due to constructive interference of phase-shifted momentum states due to this pulse as shown in Fig. 1(a). Studies of such quantum resonances with a large number of excitation pulses applied at multiples or submultiples of $T_r$ have attracted considerable attention in experiments that focus on quantum chaos [18–23]. Related work includes studies of the Talbot effect in atom optics [24–26].

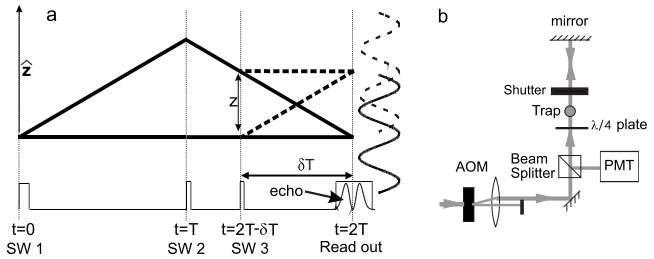


FIG. 1. (a) Recoil diagram where solid lines are momentum states differing by $2\hbar k$; dashed lines show phase-shifted trajectories due to a third standing-wave (SW) pulse applied at $t=2T-\delta T$. (b) Schematic of the experimental setup.

 

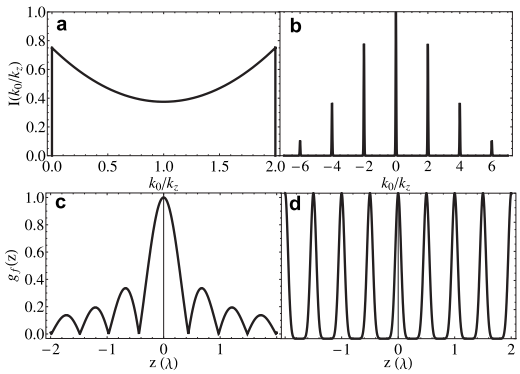


FIG. 2. (a) and (b) show $I(k_0)$ for traveling-wave and standing-wave pulses, respectively. (c) and (d) show associated $g_f(z)$.

In this work, we use a coherence function [11] that is a Fourier transform of the momentum distribution associated with the third pulse to describe the periodic contrast. If the third pulse is a traveling wave, the quasiperiodic contrast cannot be fully recovered due to decoherence from spontaneous emission. However, the contrast can again be described using a coherence function as in beam experiments [7–10].

We now describe the theoretical formalism based on the one-dimensional coherence function [7–11] used to describe our results. Coherence functions are Fourier transforms of the probability distributions $P(\Delta k)$ that describe a change in momentum $(\hbar\Delta k)$ associated with the third pulse and can be written in terms of the correlation between interfering momentum states separated by $z$ [see Fig. 1(a)] as

$$g(z) = \int \phi(z' - z)\phi^*(z')dz' = \mathcal{F}_z\{I(k_0)\}, \tag{1}$$

where $\phi(z)$ is the atomic wave function, $k_0$ is the initial wave vector for the atoms, and $\mathcal{F}_z$ denotes a Fourier transform of the momentum distribution of the atoms, $I(k_0)$. If a photon of wave vector $\mathbf{k}$ is absorbed and subsequently reemitted due to spontaneous emission, the final momentum distribution along the $z$ axis is given by

$$I_f(k_0) = \int dk_z I_i(k_0 - k_z)P(k_z) = I_i(k_0) * P(k_z). \tag{2}$$

The subscripts $i$ and $f$ denote initial and final distributions, respectively, and $*$ represents a convolution between the initial atomic momentum distribution and the momentum distribution $P(k_z)$ that describes photon scattering. If $I_i(k_0)$ is a delta function and $P(k_z)$ describes absorption followed by spontaneous emission for a dipole oscillating in the $x$-$y$ plane (situation for traveling-wave excitation), we obtain $I_f(k_0)$ shown in Fig. 2(a). The corresponding coherence function $g(z)$, shown in Fig. 2(c), is the Fourier transform of $I_f(k_0)$. $g(z)$ is analogous to the single-slit diffraction function in optics, which represents the contrast after a single absorption-emission process.

To describe multiple independent absorption-emission events, Eq. (2) can be used repeatedly to convolve $I_f(k_0)$ with $P(k_z)$. The convolution theorem can be used to show that the final coherence function $g_f(z)$ is a weighted sum of the single-photon coherence function $g_1(z)$ given by

$$g_f(z) = \sum_{n=0}^{\infty} c_n g_1^n(z), \tag{3}$$

where the weighting coefficients $c_n$ depend on the interaction time, intensity, and detuning of the third pulse and represent the probabilities of scattering $n$ photons.

For the case of standing-wave excitation, $I_f(k_0)$ will resemble a distribution of evenly spaced delta functions (the finite peak width is due to the uncertainty in $k$) as shown in Fig. 2(b). The corresponding $g_f(z)$ shown in Fig. 2(d) resembles the interference pattern due to multiple slits and can be represented by

$$g_f(z) = \mathcal{F}\{I_f(k_0)\} \simeq \sum_{n=0}^{\infty} c_n e^{\pm i2nk_z z}. \tag{4}$$

$c_n$ represents the probability of the atom acquiring a momentum kick of $2n\hbar k$ during excitation where $n$ is an integer. For a multislit experiment, the values of $c_n$ would be equal, whereas for the standing-wave experiment, $c_n \propto |J_n(\phi)|^2$, where $\phi$ is the standing-wave pulse area and $J_n$ is a Bessel function of order $n$. In the rest frame of atoms used in beam experiments, the effect of spatially separated laser fields is equivalent to the effect of temporally separated pulses used in this work since the separation between interfering arms that interact with the third pulse is given by $z = (2\hbar k/m)\delta T$ as in Fig. 1(a). As a result, Eq. (4) can be expressed as $g(\delta T)$, a function that is modulated at $\omega_r$.

A Ti:sapphire ring laser produces the laser beams used for atom trapping and atom interferometry. The repump laser is derived from a grating-stabilized diode laser. We use a magneto-optical trap (MOT) containing $\sim 10^8$ $^{85}$Rb atoms loaded in $\sim 100$ ms from background vapor. After turning off the trap and repump lasers, the atoms are cooled in a molasses to a temperature of $\sim 50$ $\mu$K. A chain of acousto-optic modulators (AOMs) generates all excitation pulses with an on/off ratio $R > 10^6$. The pulse timing is controlled by digital delay generators precise to 500 ps. Figure 1(b) shows a schematic of the beam path. Traveling-wave pulses from an AOM are retroreflected to produce standing-wave pulses. The excitation beam diameter is comparable to or slightly larger than the cloud size of $\sim 4$ mm. A shutter with a closing time of $\sim 600$ $\mu$s is used to block light at the time of the readout pulse. The contrast is detected using a gated photomultiplier tube (PMT). Due to the jitter in the shutter closing time, the smallest pulse separations $T$ for which the echo can be recorded is $\sim 1$ ms. For some experiments, two AOMs are used to generate counterpropagating traveling-wave pulses, in which case the shutter is eliminated and $T$ can be reduced to $\sim 1$ $\mu$s. The peak intensity of all the pulses is $I \sim 5I_{\text{sat}}$, where $I_{\text{sat}} = 7.56$ mW/cm$^2$ is the saturation intensity associated with equally populated magnetic sublevels of the $F=3$ ground state. The durations of the two AI pulses are 500–800 ns and 30–200 ns, respectively. The typical duration of the third pulse is 50–500 ns. The grating is detected using a readout pulse that has the same detuning $\Delta$ ($\sim 50$ MHz) as the AI pulses. The echo envelope shown in Fig. 1(a) is averaged over 32 repetitions and integrated over the typical signal duration ($\sim 2$ $\mu$s) to generate the grating contrast.

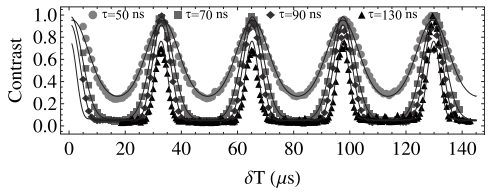


FIG. 3. Contrast vs $\delta T$ with a third standing-wave pulse with $\Delta=50$ MHz. The fits are based on Eq. (4). For $\tau=70$ ns, $c_0=0.34$, $c_1=0.43$, $c_2=0.17$, $c_3=0.04$, and $c_4=0.01$. The maximum of each curve represents complete recovery of contrast.

Figure 3 shows the effect of a third standing-wave pulse with variable pulse width $\tau$ on the contrast with $T\sim 1.5$ ms. The data are modulated at $\omega_r$ and show that 100% contrast is regained since the effect of spontaneous emission is small. These data are qualitatively similar to Fig. 2(d). The fits are based on Eq. (4) and involve a finite number of terms due to the bandwidth and pulse area of the third pulse. As expected, the fringe pattern narrows if the duration of the third pulse is increased because of interference of phase-shifted trajectories due to higher-order recoil processes. The modulated contrast suggests that this technique could be suitable for measuring $\omega_r$ precisely if $\delta T$ is varied over the time scale of the experiment ($\sim 2T$). Figure 4(a) shows such a measurement with the standing-wave pulses of the AI separated by $\sim 8$ ms. The data were acquired in $\sim 2$ h. A fit to $g_f(\delta T)$ based on Eq. (4) results in a measurement of $\omega_r$ precise to 1.6 parts per million. The contrast in Fig. 4(a) can also be analytically modeled by extending the theoretical treatment in Refs. [13,17]. In Ref. [13], the presence of higher-order density gratings was inferred by applying a sequence of standing-wave pulses and observing signatures at specific echo times. In contrast, this work describes the effect of a third pulse on the echo at $t=2T$ associated with the $\lambda/2$ spatial harmonic. Using the treatment of spontaneous emission described in Ref. [17] and the theory of echo formation using multiple pulses developed in [13], it can be shown [27] that the grating contrast in the presence of the third standing-wave pulse is given by

$$g_f(\delta T) \propto J_0[2|\phi_3|\sqrt{\sin(\omega_r \delta T+\theta)\sin(\omega_r \delta T-\theta)}]. \qquad (5)$$

Here, $\phi_3$ is the pulse area of the third pulse, $\theta=\tan^{-1}(-\Gamma/\Delta)$ is the spontaneous emission parameter, and $\Gamma$ is the effective radiative rate [17]. Figure 4(b) shows fits to the data in Fig. 4(a) based on Eq. (4) and on the results based on a modification of Eq. (5) to include the effects of the spatial profiles of the atomic cloud and laser beams. Both fits accurately model the data, but the fit based on Eq. (4) is more robust because the effect of spontaneous emission and spatial profile can be described by a modification of the weighting coefficients in the series expansion. This has been confirmed using numerical simulations. Another interesting aspect of using a third pulse to measure $\omega_r$ is that the effect of signal decay due to transit time of cold atoms is avoided because $T$ is fixed. It is notable that the technique described here is considerably simpler than the method used in Refs. [15,17], which involved measuring the periodic modulation of the contrast as a function of $T$ and developing fits based on analytical calculations that describe the role of spontaneous emission and spatial profile of the AI beams. As a result, accurate knowledge about numerous fit parameters such as pulse areas, effective spontaneous emission rate, and contrast decay time was essential.

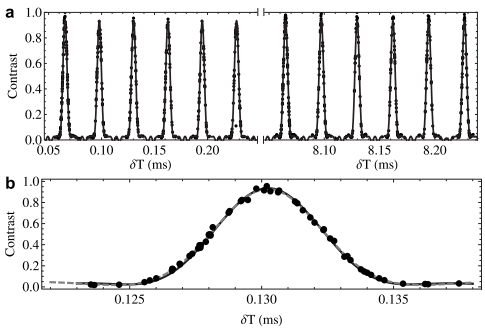


FIG. 4. (a) Measurement of $\omega_r$ using a third standing-wave pulse with duration $\tau=150$ ns. The data are fit to Eq. (4). The fit gives $\omega_r=97\,003.2\pm 0.16$ s$^{-1}$. (b) Expanded view showing fits based on Eq. (4) (solid line) and Eq. (5) (dashed line).

Analysis of the data in Fig. 3 shows that the full width at half maxima (FWHM) of the fringe pattern is inversely proportional to $\phi_3$, a result that can be derived by expanding $J_0$ in Eq. (5) around its maxima [27]. We have also examined the effect of $N$ identical standing-wave pulses separated by $T_r$ on the FWHM. The FWHM decreases with $N$ and levels off for $N\sim 7$ at $\sim 1/2$ the value for $N=1$. In comparison, a derivation following from Eq. (5) predicts a $1/N$ dependence for the FWHM for $\phi \ll 1$ [27]. We attribute the discrepancy to the relatively large pulse area used in this work ($\phi\sim 1$) and the finite bandwidth of additional pulses, effects not considered by the theoretical treatment.

The best atom interferometric measurements of $\omega_r$ [5,6] have achieved a precision better than 10 parts per billion (ppb) by studying systematic effects using multiple data sets on time scales of $\sim 200$ ms. In contrast, Fig. 4(a) is a single measurement of $\omega_r$ on a time scale of $\sim 20$ ms. This measurement does not correct for systematic effects such as angle between the traveling-wave components of the standing-wave pulse [17] and index of refraction [28], which are effects at the level of 1 ppm. In recent work, we have shown that the time scale can be further extended to the transit time limit by switching to a glass chamber and eliminating magnetic field gradients [16] due to the magnetized vacuum chamber. Since the precision scales linearly with $T$ and further improvement up to a factor of $\sim 10$ is feasible by increasing the pulse area and number of standing-wave pulses, a single measurement with a precision of $\sim 20$ ppb seems realizable. Further improvements can be achieved on the basis of statistics and studies of systematic effects. To minimize the index correction, we expect to use far detuned excitation pulses as in Refs. [6,18,19]. Other systematic effects include wave-front curvature. Pursuit of a measurement of $\omega_r$ using the single-state, echo-type AI and the coherence function technique in a dilute atomic cloud is advantageous because of reduced sensitivity to several systematic effects [15] and because recoil shifts due to interatomic interactions are avoided [29].

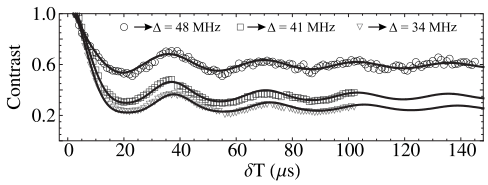


FIG. 5. Contrast vs $\delta T$ with a traveling-wave pulse with $\tau = 150$ ns perturbing the AI. The fits are based on Eq. (3). For the case of $\Delta = 34$ MHz, $c_0 = 0.16$, $c_1 = 0.35$, $c_2 = 0.47$, and $c_3 = 0.02$. This function is quasiperiodic, and the spacing between maxima is $\sim T_r = 32$ $\mu$s.

We now show the connection between this work and earlier studies in atomic beams in which the momentum state interference was perturbed by a traveling wave [7–10]. Figure 5 shows the change in contrast due to a traveling wave (third pulse) with duration $\tau = 150$ ns and variable $\Delta$ applied at $t = 2T - \delta T$ with the AI pulses separated by $T \sim 1.5$ ms. The contrast shows the modulation expected on the basis of Eq. (3), which is qualitatively similar to Fig. 2(c). It is clear that the contrast decreases if the third pulse is closer to resonance. A similar loss in contrast is observed if the duration of the third pulse is increased. The data are fit using Eq. (3) to extract $c_0, c_1, \ldots, c_n$. Since the third pulse was off resonance, the weighted average number of scattered photons per atom for each data set is generally small ($\sim 1.5$) and the loss in contrast does not approach 100%. The asymptotic offset of each curve is proportional to $c_0$, which represents the number of atoms that scattered zero photons. A detailed analysis of these results is presented elsewhere [27].

If the AI is perturbed by continuous-wave (cw) light, scattering events can occur with equal probability at any time during the experiment so that $g_f(z)$ must be averaged over $z$. Since $T \gg T_r$, atoms that scatter light will not contribute to the echo signal and the contrast will decay exponentially as a function of $T$. Figure 6(a) shows the contrast as a function of $T$ for various intensities of circularly polarized cw light. Following previous work related to atomic collisions [30], we assume that the contrast ratio with and without background light is proportional to $e^{-\gamma 2T}$ where $\gamma$ is the scattering rate

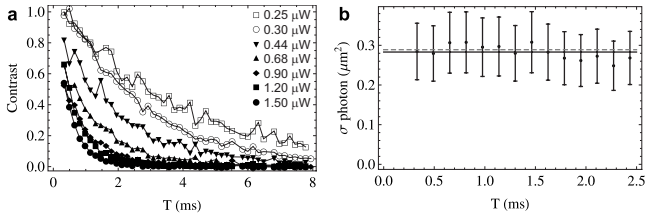


FIG. 6. (a) Contrast vs $T$ for various continuous-wave light intensities. The legend specifies the beam power. (b) $\sigma$ vs $T$. The error bars are related to uncertainties in power and spatial profile measurements, whereas the statistical uncertainties are much smaller. The solid line is the average of the data [0.28 $(\mu m)^2$], and dashed line is the expected value [0.29 $(\mu m)^2$] for a polarized sample.

(proportional to the photon density and absorption cross section $\sigma$) and $2T$ is the time of exposure to light. For fixed $T$, we find that the natural logarithm of the contrast exhibits a linear dependence on cw light intensity. $\sigma$ can be inferred from the slopes of these graphs and the measured cw light intensity. Figure 6(b) shows the cross section $\sigma$ vs $T$. As expected, $\sigma$ is independent of $T$ because photon scattering imparts a velocity change of $\hbar k/m$ ($\sim 0.6$ cm/s) that decoheres the atoms on a time scale of $\sim 1/\omega_r$. $\sigma_{\mathrm{avg}}$ is consistent with the expected value for a polarized sample $(3\lambda^2/2\pi)$ since the echo signal from the $m_f = 3$ sublevel is the dominant contribution and because a large fraction of atoms accumulate in the high-$|m|$ magnetic sublevels of the $F = 3$ state during polarization gradient cooling [16].

In summary, we have explored the distinct effects of perturbing the AI with standing-wave, traveling-wave, and continuous-wave light. The contrast relevant to standing-wave excitation has been accurately modeled using coherence functions. This technique offers a surprisingly simple and robust method to measure $\omega_r$, which can be exploited for a precise determination of $\alpha$.

This work was supported by the Canada Foundation for Innovation, Ontario Innovation Trust, Natural Sciences and Engineering Research Council, Ontario Centers of Excellence, and York University. Helpful discussions with Paul Berman, Marko Horbatsch, and Eric Hessels are acknowledged.

[1] P. L. Gould *et al.*, Phys. Rev. Lett. **56**, 827 (1986).
[2] A. Peters *et al.*, Nature (London) **400**, 849 (1999).
[3] J. M. McGuirk *et al.*, Phys. Rev. A **65**, 033608 (2002).
[4] D. S. Weiss *et al.*, Phys. Rev. Lett. **70**, 2706 (1993).
[5] A. Wicht *et al.*, Phys. Scr. **T102**, 82 (2002).
[6] P. Cladé *et al.*, Phys. Rev. Lett. **96**, 033001 (2006).
[7] T. Pfau *et al.*, Phys. Rev. Lett. **73**, 1223 (1994).
[8] M. S. Chapman *et al.*, Phys. Rev. Lett. **75**, 3783 (1995).
[9] D. A. Kokorowski *et al.*, Phys. Rev. Lett. **86**, 2191 (2001).
[10] H. Uys *et al.*, Phys. Rev. Lett. **95**, 150403 (2005).
[11] L. Mandel, J. Opt. (Paris) **10**, 51 (1979).
[12] S. B. Cahn *et al.*, Phys. Rev. Lett. **79**, 784 (1997).
[13] D. V. Strekalov *et al.*, Phys. Rev. A **66**, 023601 (2002).
[14] M. Weel and A. Kumarakrishnan, Phys. Rev. A **67**, 061602(R) (2003).
[15] M. Weel *et al.* (unpublished).
[16] M. Weel *et al.*, Phys. Rev. A **73**, 063624 (2006).
[17] S. Beattie *et al.*, Phys. Rev. A **77**, 013610 (2008).
[18] A. Tonyushkin *et al.*, e-print arXiv:0803.4153.
[19] S. Wu *et al.*, e-print arXiv:0801.0475.
[20] S. Wimberger *et al.*, Phys. Rev. Lett. **94**, 130404 (2005).
[21] C. Ryu *et al.*, Phys. Rev. Lett. **96**, 160403 (2006).
[22] M. F. Andersen *et al.*, Phys. Rev. Lett. **97**, 104102 (2006).
[23] F. L. Moore *et al.*, Phys. Rev. Lett. **75**, 4598 (1995).
[24] W. H. Oskay *et al.*, Opt. Commun. **179**, 137 (2000).
[25] M. B. d'Arcy *et al.*, Phys. Rev. Lett. **87**, 074102 (2001).
[26] A. Turlapov *et al.*, Phys. Rev. A **71**, 043612 (2005).
[27] S. Beattie *et al.* (unpublished).
[28] G. Campbell *et al.*, Phys. Rev. Lett. **94**, 170403 (2005).
[29] S. Gupta *et al.*, Phys. Rev. Lett. **89**, 140401 (2002).
[30] T. W. Mossberg *et al.*, Phys. Rev. Lett. **44**, 73 (1980).